AIP | Physics of Fluids

Multiscale modeling of particle in suspension with smoothed dissipative particle dynamics

Xin Bian, Sergey Litvinov, Rui Qian, Marco Ellero, and Nikolaus A. Adams

Citation: Phys. Fluids **24**, 012002 (2012); doi: 10.1063/1.3676244
View online: http://dx.doi.org/10.1063/1.3676244
View Table of Contents: http://pof.aip.org/resource/1/PHFLE6/v24/i1
Published by the American Institute of Physics.

Multiscale modeling of particle in suspension with smoothed dissipative particle dynamics

Xin Bian,[a] Sergey Litvinov, Rui Qian, Marco Ellero, and Nikolaus A. Adams
Lehrstuhl für Aerodynamik und Strömungsmechanik, Technische Universität München, Boltzmannstr. 15, D-85748 Garching bei München, Germany

(Received 18 April 2011; accepted 30 November 2011; published online 19 January 2012)

We apply smoothed dissipative particle dynamics (SDPD) [Español and Revenga, Phys. Rev. E **67**, 026705 (2003)] to model solid particles in suspension. SDPD is a thermodynamically consistent version of smoothed particle hydrodynamics (SPH) and can be interpreted as a multiscale particle framework linking the macroscopic SPH to the mesoscopic dissipative particle dynamics (DPD) method. Rigid structures of arbitrary shape embedded in the fluid are modeled by frozen particles on which artificial velocities are assigned in order to satisfy exactly the no-slip boundary condition on the solid-liquid interface. The dynamics of the rigid structures is decoupled from the solvent by solving extra equations for the rigid body translational/angular velocities derived from the total drag/torque exerted by the surrounding liquid. The correct scaling of the SDPD thermal fluctuations with the fluid-particle size allows us to describe the behavior of the particle suspension on spatial scales ranging continuously from the diffusion-dominated regime typical of sub-micron-sized objects towards the non-Brownian regime characterizing macro-continuum flow conditions. Extensive tests of the method are performed for the case of two/three dimensional bulk particle-system both in Brownian/non-Brownian environment showing numerical convergence and excellent agreement with analytical theories. Finally, to illustrate the ability of the model to couple with external boundary geometries, the effect of confinement on the diffusional properties of a single sphere within a micro-channel is considered, and the dependence of the diffusion coefficient on the wall-separation distance is evaluated and compared with available analytical results. © *2012 American Institute of Physics*. [doi:10.1063/1.3676244]

I. INTRODUCTION

Particles suspended in a solvent matrix represent a common scenario embracing physical processes that occur at different spatial scales, ranging from macroscopic scale (on the order of millimeters and larger) typically found in processing engineering down to the sub-micron scale characterizing micro/nano-fluidics.

The modeling of particle suspensions is not only important to improve our understanding of the bulk rheological properties of complex particulate materials, a topic which is still subject of intense research[1] and industrial interest,[2] but also becoming an indispensable tool to target/optimize specific functionalities of novel devices operating under microfluidics conditions.[3,4] Manipulation/sorting/mixing of micro/nano-size objects is becoming the central focus of nanoparticle technology as well as, in the biomedical field, of novel platforms for hand-held diagnostics.[5] It is, therefore, extremely important to develop simultaneously theoretical and numerical models to fill the gap with rapidly evolving industrial applications.

Modeling of particle suspensions based on non-Brownian continuum approaches has often been proposed in the past using several grid-based techniques, such as finite elements methods,[6] distributed Lagrange-multiplier-based fictitious-domain methods (DLM)[7,8] and smoothed profile methods (SPM),[9,10] to mention but a few. These approaches are very useful but they rely on a

[a]Electronic mail: xin.bian@aer.mw.tum.de.

deterministic discretization of the hydrodynamic equations and are, therefore, limited to large Péclet number (defined as ratio of shear rate and mass diffusion) flow of supra-micron-sized particle suspensions. In several microflow conditions, the thermal noise, which manifests itself as the diffusional motion of the suspended objects, plays a key role in the dynamics. For example, an accurate description and measurement of the diffusion motion of a colloidal particle may be used as a highly sensitive probe for structure properties, both in distance and orientation, in the presence of complex boundaries.[11,12] Therefore, it is crucial to incorporate it into the adopted formalism.

Conventional schemes for the simulation of Brownian suspensions include a stochastic thermal force explicitly applied on the suspended bead while the effect of the hydrodynamic interactions (HIs) among them is implicitly taken into account via Oseen tensor-based models or higher-order expansions of the incompressible Stokes equations. Afterwards, a resulting set of algebraical equations need to be inverted. These approaches include, for example, Brownian dynamics (BD)[13] and Stokesian dynamics (SD).[14,15] Their main advantage is related to the good scalability of the number of equations with the number of suspended particles, allowing for the simulation of very large systems.[16] On the other hand, SD assumes that the time scales between the motions of fluid and those associated with particles are completely separated, which excludes the short-time motion of Brownian particles over kinematic time scale. Moreover, modeling arbitrarily shaped objects and complex boundary geometries is not an easy task and requires essential modification of the standard framework.[17] Generalization of SD to model nonspherical particles has been recently proposed in Ref. 18. In this approach, arbitrarily shaped rigid particles are modeled as clusters of several spheres which still interact via the usual SD forces, therefore, extending its range of applicability while increasing computational cost. Another approach which allows the simulations of arbitrarily shaped particles is based on boundary integral analysis.[19] Here, particle surfaces are discretized and a set of boundary integral equations based on the expansion of the Stokes equations must be solved for each surface element.

The direct numerical simulation (DNS) methods mentioned at the beginning of this section do not require any explicit model of the hydrodynamic interactions among particles being the solvent dynamics fully discretized. In order to be applied to microflow conditions, they need to be generalized. In Ref. 20, thermal fluctuations have been incorporated in an Eulerian finite volume scheme by including them in the discretized momentum equations by a random stress term equivalent to the fluctuating hydrodynamic equations of Landau and Lifshitz.[21] In this approach, the Brownian motion of a suspended object is implicitly induced by the thermal agitation of the solvent fluid and does not need to be modeled. A similar approach was previously applied also to lattice-Boltzmann (LB) simulation by Ladd and his coworker,[22,23] where a random stress term was introduced in the LB equation. A problem occurring in the LB simulations of suspended particles is, however, related to their unclear size which is not known *a priori*. One needs, therefore, to calibrate the simulations with a so-called hydrodynamic radius,[24] which can, however, be a complex function of the lattice size,[25] as well as the solvent kinematic viscosity.[26] Recently, some of these deficiencies have been significantly reduced by employing multiple relaxation time (MRT) approaches[26] or higher-order boundary conditions.[27] Similar to SD method, thermal fluctuations have been directly introduced on particles instead of fluid for SPM method, which was used to study diffusive behavior of Brownian spherical particles.[28,29] This poses again a potential difficulty for the simulation of nonspherical Brownian particles.

Another popular method which incorporates thermal noise is dissipative particle dynamics (DPD).[30] This represents a grid-off method in which the elements of fluid are modeled by particles interacting via soft conservative, frictional, and stochastic forces, the latter ones being related to the dissipative via the fluctuation-dissipation theorem (FDT).[31] The method is flexible, allowing for modeling arbitrarily shaped rigid structures by simply freezing DPD particles located inside the solid domain and letting them interact with the fluid particles.[30,32] It has been used to investigate the rheology of colloidal suspension under semi-dilute/concentrated flow conditions in Refs. 33 and 34. Recently, good results have been also obtained by simulating colloidal particles as single DPD particles interacting with the solvent ones via the ordinary DPD forces and among them with extra colloid-colloid interactions.[35,36] Although the results are qualitative and restricted to spherical particles only, the authors were able to simulate large concentrated systems and obtain the typical shear-thinning behavior observed experimentally.

Despite the good performance of DPD in simulating complex systems, the method still suffers of some shortcomings. The price for the simplicity of DPD is related to the lack of direct connection between the model parameters and the physical parameters of the system one tries to simulate. Usually, to specify the fluid transport coefficient, one needs to rely on kinetic theory[37] or map and calibrate the parameters in ways that are not always systematic.[38,39] Perhaps, the most serious problem is the specification of the spatial scale at which a DPD simulation operates, posing some difficulties on the separate identification of resolution and finite-size effects in the output results.[33,40] In particular, there is no unique definition of the hydrodynamic fluctuations acting on the fluid elements. The previous drawbacks have been addressed and solved in a modification of DPD (Ref. 41) denoted as smoothed dissipative particle dynamics (SDPD). The new particle model is entirely embedded in the GENERIC framework;[42,43] therefore, it maintains the thermodynamic consistency of the original DPD method, but in addition allows for a direct specification of the transport coefficient, i.e., viscosity, as input parameter. In fact, it has been shown that SDPD represents a generalization of the well-known smoothed particle hydrodynamics (SPH) which is a Lagrangian meshless Navier-Stokes solver proposed by Monaghan,[44,45] albeit with consistent introduction of thermal fluctuations.[46]

A remark on the amount of thermal fluctuations introduced in SDPD is in order. The scaling of SDPD thermal fluctuations with the fluid particle size has been investigated in Ref. 47 where it has been shown that their magnitude increases as the inverse of the square root of the fluid particle volume, in agreement with classical results in statistical mechanics. Therefore, whenever the fluid particle size is large enough, no thermal noise will be present in the hydrodynamic variables, whereas it will show up when the fluid description needs to be miniaturized, e.g., in microflow conditions. It is remarkable that the application of GENERIC together with a form of the dissipative terms taken from SPH allows for defining uniquely a size-dependent thermal noise which satisfies the FDT. The method has been recently applied to simulations of polymer molecules in suspension,[48,49] multiphase flows,[50] and viscoelastic liquids.[51]

In this paper, we present a multiscale model of arbitrarily shaped particle suspension based on SDPD which is able to operate on different flow conditions ranging continuously from the diffusion-dominated regime typical of micro/nano-sized objects to the non-Brownian regime typical of supra-micron-size particles. Moving rigid structures are modeled by freezing SDPD particles within the solid domain and letting them interact with the fluid particles. Artificial boundary velocities are assigned to the frozen solid boundary particles during the interaction with the fluid particles following Ref. 52, which allows for enforcing exactly the no-slip boundary condition on the solid-liquid interface.

The strict connection of the SDPD method to SPH enables us to investigate resolution effects in the Brownian regime by applying standard continuum convergence analysis to the results. The resolution studies and exact quantitative comparison in a Brownian environment are crucial, for example, to investigate the effect of particle-shape on microrheology which is based on many-points particle correlation measurements[53] and which represents our long-term research goal.[51]

The paper is organized as follows: Sec. II describes the deterministic and stochastic SDPD model of the solvent as well as the specific model of the rigid suspended structures and their interaction with the fluid. Numerical results of the particle-suspension model based on a strict convergence analysis under both non-Brownian and Brownian conditions are presented in Sec. III. Finally, conclusions and further developments are discussed in Sec. IV.

II. THE PARTICLE MODEL

A. Lagrangian hydrodynamic equations

Let us consider the isothermal Navier-Stokes equations in a Lagrangian framework,

$$\frac{d\rho}{dt} = -\rho \nabla \cdot \mathbf{v}, \tag{1}$$

$$\frac{d\mathbf{v}}{dt} = -\frac{\nabla p}{\rho} + \mathbf{F} + \mathbf{g}, \tag{2}$$

where ρ, $\mathbf{v}$, p, $\mathbf{F}$, and $\mathbf{g}$ are material density, velocity, pressure, viscous force, and body force, respectively. Following earlier studies of quasi-incompressible flow modeling,[54–56] an equation of state relating pressure to density can be written as

$$p = p_0\left[\left(\frac{\rho}{\rho_r}\right)^{\gamma} - 1\right], \tag{3}$$

where p_0 (related to sound speed c_s), $\gamma = 7$, and ρ_r are parameters chosen based on a scale analysis[52,55] such that pressure field reacts strongly to small derivations in mass density and quasi-incompressibility is enforced. Assuming Newtonian flow, the viscous force $\mathbf{F}$ simplifies to

$$\mathbf{F} = \nu\nabla^2\mathbf{v}, \tag{4}$$

where ν is the kinematic viscosity related to dynamic viscosity by $\nu = \eta/\rho$.

B. Deterministic solvent modeling

Equations (1) and (2) can be discretized in space by using the SPH method. The essence of SPH is an interpolation process allowing any function defined on a given domain to be expressed in terms of values at a discrete set of N disordered points—the particles.[44] Equation (1), the conservation of mass, is automatically satisfied if particle density is evaluated as[41]

$$d_i = \sum_j W_{ij}, \tag{5}$$

where $d_i = 1/\mathcal{V}_i$ is the number density associated to particle i, and $\mathcal{V}_i$ the corresponding volume. Accordingly, the mass density is evaluated as $\rho_i = m_i d_i$, where m_i is the mass of particle i; $W_{ij} = W(r_{ij}, h)$ is an even, bell shaped weighting function with smoothing length h, where $r_{ij} = |\mathbf{r}_i - \mathbf{r}_j|$ is the distance between particle i and j. For this work, we use a quintic spline[52] kernel characterized by a compact support with cutoff radius $r_c = 3h$.

Application of the SPH approximation to Eq. (2) produces the following equations for the particle positions and momenta:[41,50]

$$\dot{\mathbf{r}}_i = \mathbf{v}_i, \tag{6}$$

$$m_i\dot{\mathbf{v}}_i = -\sum_j\left(\frac{p_i}{d_i^2} + \frac{p_j}{d_j^2}\right)\frac{\partial W}{\partial r_{ij}}\mathbf{e}_{ij} + \sum_j \eta\left(\frac{1}{d_i^2} + \frac{1}{d_j^2}\right)\frac{\partial W}{\partial r_{ij}}\frac{\mathbf{v}_{ij}}{r_{ij}} + \mathbf{g}_i. \tag{7}$$

In the following, we will consider constant particle masses $m_i = m_0$ ($\forall i = 1, \ldots, N$). The first part on the rhs of the momentum equation represents a pressure force acting along the unit vector $\mathbf{e}_{ij} = \mathbf{r}_{ij}/r_{ij} = (\mathbf{r}_i - \mathbf{r}_j)/|\mathbf{r}_{ij}|$ joining particles i and j. Since it is a central force and symmetric by interchanging particle indices, total linear and angular momenta are exactly conserved. The irreversible viscous force is calculated in the second term of the rhs in Eq. (7) to reduce velocity differences between pair of particles. This force is symmetric by interchanging particle indices; therefore, it conserves linear momentum strictly. However, it is non-central, providing only approximate conservation of angular momentum.[41] The third term describes an external body force $\mathbf{g}_i$ as, for example, the gravity.

The SPH equations represent a discretization of the deterministic Newtonian hydrodynamics performed on Lagrangian elements of fluid.

C. Stochastic solvent modeling: Thermal fluctuations

Micro/nano-scopic flow problems are characterized by the presence of thermal fluctuations in the hydrodynamic variables. It was shown[41] that the GENERIC framework[42,43] allows for incorporating particle-fluctuations into Eq. (7) in a thermodynamically consistent way. In particular, the fluctuations of the momentum of particle i caused by thermal noise for an isothermal incompressible fluid are simply

$$d\widetilde{\mathbf{P}}_i = \sum_j \left[-4k_B T\eta \left(\frac{1}{d_i^2} + \frac{1}{d_j^2} \right) \frac{1}{r_{ij}} \frac{\partial W}{\partial r_{ij}} \right]^{1/2} d\overline{\overline{\mathbf{W}}}_{ij} \cdot \mathbf{e}_{ij}, \tag{8}$$

where k_B is the Boltzmann constant and T is the temperature; $d\overline{\overline{\mathbf{W}}}_{ij}$ is the traceless symmetric part of a matrix of independent increments of a Wiener process $d\mathbf{W}_{ij} = d\mathbf{W}_{ji}$, i.e., $d\overline{\overline{\mathbf{W}}}_{ij} = \left(d\mathbf{W}_{ij} + d\mathbf{W}_{ij}^T \right)/2 - tr[d\mathbf{W}_{ij}]\mathbf{I}/d$, where d is the spatial dimension.[41,50] Particle-velocity statistics satisfy the Maxwell-Boltzmann distribution, and their variance is given by[47]

$$\langle v^2 \rangle = d\frac{k_B T}{\rho_0 \mathcal{V}_i}, \tag{9}$$

where ρ_0 is the equilibrium fluid density. Thus, velocity fluctuations emerge naturally and increase in magnitude following the correct scaling as the spatial scales of the problem, i.e., the particle volumes $\mathcal{V}_i$, become smaller.[47]

The introduction of the term in Eq. (8) into the particle momentum equation corresponds to the so-called smoothed dissipative particle dynamics method. SDPD allows for extending the applicability of the SPH method to micro/nano scales. Unlike standard mesoscopic methods where finite-size/resolution effects are difficult to control,[33,40] the strict connection with SPH enables SDPD to perform numerical convergence studies in a Brownian environment by using established SPH error analysis,[56,57]; on the other hand, whenever the physical scale of the problem ranges in the macroscopic scale, it reduces to a version of SPH by setting $T = 0$.

D. Modeling of a suspended solid particle

To model moving solid objects suspended in the fluid domain, one must be able to enforce the no-slip velocity boundary condition on any, possibly arbitrary, solid-liquid interface. This can be achieved by using the following strategy: initially, all SDPD particles are placed on regular lattice with distance $dx = dy(= dz)$ throughout the entire computational domain (solid and liquid). Once a given object geometry is prescribed, we can detect all the SDPD particles lying inside the solid domain B and identify them as *solid boundary particles*; the remaining ones are identified as *fluid particles*, and their evolution of hydrodynamic properties is determined from Eqs. (6)–(8). Solid boundary particles interact with fluid particles by the same Eqs. (7) and (8). However, unlike the fluid particles, their properties are not prescribed in terms of an evolution equation but must be assigned to enforce the correct conditions on the interface.

In the pioneering works on DPD modeling of colloidal suspensions,[32,33] particles inside a solid domain are "frozen" and their velocities are assigned to be equal to the rigid body motion of the modeled structure. However, this choice introduces a zero-order no-slip boundary condition and leads to an ill-defined effective structure surface at moderate resolution. To guarantee better no-slip condition at the surface of the solid object, we extend the work of Morris *et al.*[52] to describe translation, rotation, and more general shapes of solid particles.

In the following, a solid particle is considered neutrally buoyant with density equal to the equilibrium solvent density ρ_0. During the simulation, its density is kept constant, and so is its mass ($M_C = \rho_0 \mathcal{V}_C$), while density of solvent may slightly fluctuate. Let us assume that the solid particle with center location $\mathbf{R}_C$ is translating with velocity $\mathbf{V}_C$ and rotating with angular velocity Ω_C. Before the velocity-dependent viscous force calculation between a solvent particle f and a boundary particle b, an artificial velocity must be assigned to b which will result in an effective no-slip condition on the surface. The artificial velocity is calculated as follows (schematic illustration in Fig. 1): the normal distance d_f from f to the surface point s is calculated, from which the tangent plane (a line in two dimensions) $\mathbf{l}_s$ is defined. Afterwards the normal distance d_b from b to $\mathbf{l}_s$ is calculated. An artificial velocity on particle b is extrapolated from the known velocity of particle f assuming zero relative velocity on the tangent plane, that is,

$$\mathbf{v}_b = -(d_b/d_f)\left(\mathbf{v}_f - \mathbf{v}_s\right) + \mathbf{v}_s, \tag{10}$$

where $\mathbf{v}_s = \mathbf{V}_C + \Omega_C \times (\mathbf{r}_s - \mathbf{R}_C)$ and $\mathbf{r}_s$ is the position vector of point s.

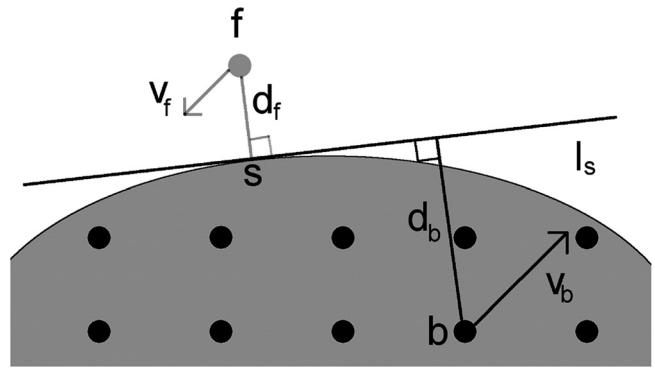

FIG. 1. A convex portion of a solid particle: f is a fluid particle and b is a boundary particle; s is the closest point on the surface to f and $\mathbf{d}_f \perp \mathbf{l}_s$, $\mathbf{d}_b \perp \mathbf{l}_s$; artificial velocity $\mathbf{v}_b = -(d_b/d_f)(\mathbf{v}_f - \mathbf{v}_s) + \mathbf{v}_s$ is used for viscous, stochastic force calculation.

s is always calculated as the closest point to fluid particle f. A distinction between convex and concave surfaces, as suggested in Ref. 52 was found to be unnecessary. For both convex and concave surfaces, the cutoff r_c should be at least smaller than the smallest surface curvature radius to have a converged result (in this article, convergence means that with a fixed number of neighboring particles, relevant results do not change as the total number of particles increases, see Sec. III). Note that $\mathbf{v}_b$ is not used to integrate boundary particle position but to enforce the correct interpolation only.

Assuming that the boundary particle b has the same viscosity η and temperature T as the solvent particle f, viscous and stochastic forces between particles b and f can be evaluated. Concerning the pressure boundary condition, we consider a Neumann condition with zero derivative between a fluid particle and a boundary particle, i.e., by linear approximation $p_b = p_f$, which allows to determine the pairwise pressure force in Eq. (7). Boundary particles are treated in the same way as solvent particles for the pair force calculation, except that two boundary particles belonging to the same structure do not interact with each other.

The procedure is repeated for every particle pair (b,f). Once all pair interactions involving b have been calculated, a total force $\mathbf{F}_b$ on b is summed up. Finally, a total force exerted by the surrounding solvent particles on the entire solid object can be obtained as $\mathbf{F}_C = \sum_{b\in B} \mathbf{F}_b$, where B is the domain occupied by the solid object. Accordingly, the translational acceleration of the solid particle is $\mathbf{a}_C = \mathbf{F}_C/M_C$. Similarly, a total torque on the solid can be calculated as $\tau_C = \sum_{b\in B} (\mathbf{r}_b - \mathbf{R}_C) \times \mathbf{F}_b$, and its angular acceleration is evaluated as $\alpha_C = \tau_C/I_C$, where I_C is momentum of inertia of the solid.

In practice, boundary particles do not fill the entire structure but are considered only within a thin layer of width r_c inside the surface of the solid. This choice saves computational time, especially for concentrated suspensions where the number of boundary particles can become comparable to the fluid ones. The same approach discussed above can be applied also to the modeling of arbitrary solid walls with random boundary particle distributions, which has been shown to reproduce better the mechanical properties of nano-systems.[49]

E. Time integration

An explicit modified velocity Verlet algorithm with $\lambda = 1/2$ is used as time integrator for solvent particles,[58]

$$\begin{aligned}
\widetilde{\mathbf{v}}_i(t+\Delta t) &= \mathbf{v}_i(t) + 1/2\Delta t \mathbf{f}_i(t),\\
\mathbf{r}_i(t+\Delta t) &= \mathbf{r}_i(t) + \Delta t \widetilde{\mathbf{v}}_i(t+\Delta t),\\
\mathbf{f}_i(t+\Delta t) &= f_i(\mathbf{r}(t+\Delta t), \widetilde{\mathbf{v}}(t+\Delta t)),\\
\mathbf{v}_i(t+\Delta t) &= \widetilde{\mathbf{v}}_i(t+\Delta t) + 1/2\Delta t \mathbf{f}_i(t+\Delta t),
\end{aligned} \tag{11}$$

where by predicting velocity before updating position, $\widetilde{\mathbf{v}}$ does not need to be stored, as it can occupy the same memory location as $\mathbf{v}$.

Some pioneers of DPD used $\widehat{\mathbf{v}}_b = V_C + (\mathbf{r}_b - \mathbf{R}_C) \times \Omega_C$ to update each solid-boundary-particle position at every time step. However, when the tangential component $(\mathbf{r}_b - \mathbf{R}_C) \times \Omega_C$ is multiplied by a finite Δt, the particle trajectory can cause an artificially expanding solid structure, which causes numerical instability. We have followed Ref. 59 and used a rotation matrix to track rotational solid structure. Both translational and rotational motions of a solid particle are updated using the same time integrator as solvent particles.

To maintain numerical stability of the explicit scheme, the time-step size Δt must be restricted by two conditions:[52] $\Delta t \leq (1/8)h^2/\nu$ and $\Delta t \leq (1/4)h/c_s$. For deterministic low Reynolds number flow problems with large resolutions, the viscous constraint is usually the dominating criterion.[52] However, in flow problems where the Brownian motion is important, the Courant-Friedrichs-Lewy (CFL) condition[60] may be the most strict limitation.

III. NUMERICAL RESULTS

In this section, we validate the SDPD model for suspended particles. A parallel version of the SDPD algorithm has been implemented using the parallel particle mesh (PPM) library[61] Non-Brownian test cases include: (1) flow through porous media, (2) dynamics of an isolated impulsively started solid particle, (3) a rotating particle under shear flow, and (4) hydrodynamic interactions between two approaching spheres; validation under Brownian conditions are considered by studying the translational/rotational diffusive behavior of a neutrally-buoyant rigid particle suspended in a solvent medium with periodic boundaries and anisotropic diffusion of a rigid particle near a planar wall.

In non-dimensional units, the solid particle radius R_C and equilibrium density ρ_0 are both equal to one. Simulations start with SDPD particles initially placed on a square (cubic) lattice with distance $dx = dy(= dz)$.

For deterministic simulations, the typical velocity V (either inflow velocity or solid particle's velocity) has the value of unity. Therefore, time has unit of R_C/V. A smoothing length $h = \kappa dx$ with $\kappa = 1.6$ (2D) or $\kappa = 1.33$ (3D), corresponding to an average number of neighboring particles of approximately 70 or 250, is adopted.

For Brownian simulations, the input energy $k_BT = 1$. Therefore, the velocity has unit of $\sqrt{k_BT/M_C}$ and time has unit of $R_C/\sqrt{k_BT/M_C}$. $\kappa = 1.0$ is universally used in both 2D and 3D simulations, corresponding to an average number of neighbors equal approximately to 27 and 106, respectively.

The speed of sound c_s is chosen to be at least 10 times larger than the typical velocity to keep fluid density variations reasonably small,[55] to balance pressure, viscous, and body forces,[52] and to satisfy time scale separation[62] (sonic time τ_c much smaller than viscous time τ_ν, i.e., $R_C/c_s \ll R_C^2/\nu$).

A. Flow through porous media

As the first test case, we consider the flow through a square/cubic periodic array of fixed circular/spherical objects. Hasimoto[63] derived an analytical expression of the drag coefficients for dilute arrays of disks and spheres by solving the Stokes equations of motion in Fourier space. Later, Sangani and Acrivos[64] extended Hasimoto's expressions to the semi-dilute case by including higher-order terms. In the two-dimensional case, the drag coefficient λ_{2D} is

$$\frac{F}{\eta V} = 4\pi\left[-\frac{1}{2}\ln C - 0.738 + C - 0.887C^2 + 2.039C^3 + O(C^4)\right]^{-1}, \tag{12}$$

where F is the drag on the disk, V is a far-field velocity, and $C = \pi R_C^2/L^2$ is the disk concentration. SDPD simulations have been performed with kinematic viscosity $\nu = 41.67$, maximum chosen sound speed $c_s = 2000$, and temperature $T = 0$ (non-Brownian regime). A fixed disk radius $R_C = 1.0$ is considered while different box lengths L are used to obtain different concentrations C. An inflow velocity $V = 1.0$ is chosen which defines a Reynolds number $\mathrm{Re} = VR_C/\nu \approx 0.024$ and a Mach number $\mathrm{Ma} = V/c_s = 5.0 \times 10^{-4}$.

By fixing the kernel overlap ($r_c = 3h = 4.8dx$) and changing resolutions (total number of particles), converged results were achieved according to the resolutions given in Table I. By increasing

TABLE I. Converged resolutions used in the simulation of flow through array of disks: $dx = dy$, $N_x = N_y$.

L	**15.0**	**7.5**	**5.0**	**4.0**	**3.5**	**3.0**	**2.7**	**2.5**	**2.3**	**2.2**
dx	0.1	0.1	0.1	0.05	0.0357	0.03125	0.025	0.02	0.0115	0.0088
N_x	150	75	50	80	98	96	108	125	200	250

L, the only constraint on resolution was the geometry of disk, which did not change. Therefore, resolutions are the same in Table I for box lengths $L \geq 5.0$. It has been suggested previously that, to obtain converged results, each pore throat/gap should be spanned by at least 15 fluid particles.[65] Therefore, when decreasing L, the number of particles in the gap between disks should be kept around 15.

Sangani and Acrivos[64] obtained a two-dimensional "lubrication approximation" for λ_{2D} in concentrated cases,

$$\frac{F}{\eta V} = \frac{9\pi}{2\sqrt{2}}\left[1 - \left(\frac{C}{C_{max}}\right)^{1/2}\right]^{-5/2}, \tag{13}$$

where the highest packing ratio is estimated as $C_{max} = \pi(R_C)^2/(2R_C)^2 \approx 0.785$ in the case of a square array of disks. Concentrated case up to $C = 0.649$ has been simulated and converged results obtained with the resolutions given in Table I. For $C = 0.649$, the total number of particles according to the converged resolution should be $N = N_x \times N_y = 250^2 = 62\,500$. However, the thin-layer surface model for the disk (see Fig. 2) allow to reduce N to 25 424 which reduces the number of particles of 60%. The thin-layer model becomes clearly even more effective in a concentrated three-dimensional system where the volume occupied by the solid objects increases as R_c^3.

Converged results for the drag coefficient are shown in Fig. 3, where good agreement with analytical theories and the two-dimensional direct DNS of Sangani and Acrivos[64] are achieved.

According to Table II, three-dimensional simulations of spheres for concentrations ranging from the dilute to semi-dilute regime have also been performed and again λ_{3D} compared with the theory of Sangani and Acrivos,[66] which in this case reads

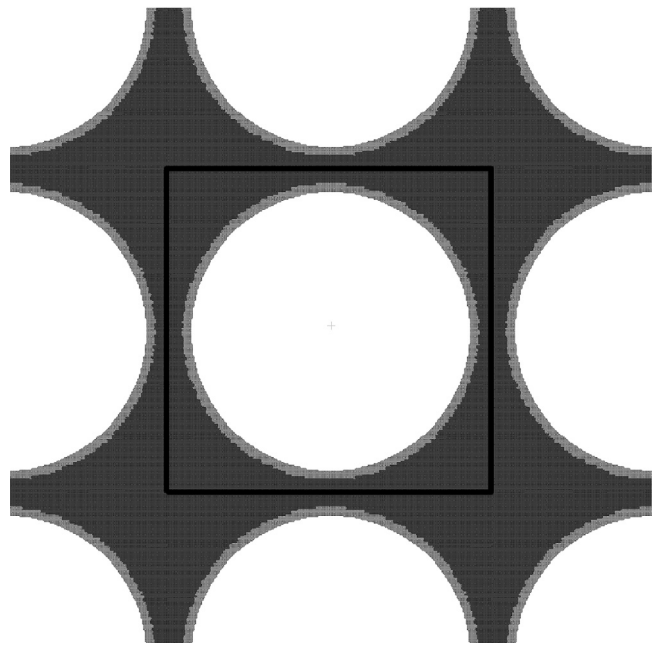

FIG. 2. A square periodic array of disks at the maximal concentration $C_{max} = 0.649$ simulated: light color are boundary particles and dark color are solvent particles. Number of particles used for converged results was $N = 25424$ while N could have been 62 500 without thin-layer model. Simulation was performed only within the black square box with periodic boundary conditions applied at its boundaries.

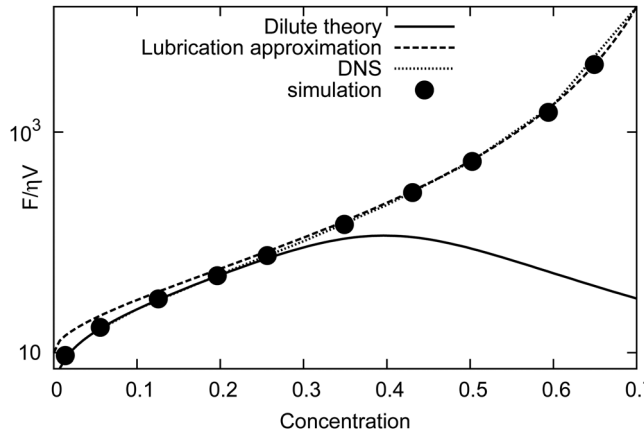

FIG. 3. Two-dimensional dimensionless drag coefficient: comparison with theories and DNS of Sangani and Acrivos.[64]

$$\frac{F}{6\pi\eta RV} = [1 - 1.7601C^{1/3} + C - 1.5593C^2 + 3.9799C^{8/3} - 3.0734C^{10/3} + O(C^{11/3})]^{-1}, \quad (14)$$

where the spheres concentration is $C = 4\pi R_C^3/3L^3$. The comparison of the converged simulation results with Eq. (14) is shown in Fig. 4, and again good agreement is achieved.

As shown from the 2D/3D drag coefficients above, the improvement on the no-slip boundary condition adopted gives effective hydrodynamic radius R_H equal to the input R_C even at moderate resolution. We have simulated problem described above also with frozen boundary particles (results not shown), i.e., without interpolation for the boundary particle velocity: the convergence of drag on the disk/sphere is much slower; therefore, $R_H \neq R_C$, similar to LB method.

B. Impulsively started non-Brownian particle

To test our particle model under unsteady situations, we have considered a circular/spherical particle moving in a Newtonian fluid. The fluid is initially at rest with kinematic viscosity $\nu = 20.0$, $c_s = 100.0$, and $T = 0$. A square(2D)/cubic(3D) computational domain with length L is considered with periodic boundary conditions applied in every direction. $L = 30$ is chosen to approximate the limiting case of an infinite solvent medium and to eliminate artificial effects due to the presence of periodic images.

At time $t = 0$, a velocity $V_C(t = 0) = V_0 = 1.0$ is assigned to the solid particle which approximates a Stokes flow, the corresponding Reynolds number is $\mathrm{Re} = R_C V_0/\nu = 0.05 \ll 1$ and Mach number is $\mathrm{Ma} = 0.01 \ll 1$.

We monitor the particle-velocity decay $V(t)$ as a function of time in the reference frame of the total system's center of mass, i.e., $V(t) = (V_C(t) - V_{CM})/(V_0 - V_{CM})$, where V_{CM} is the velocity for center of total mass. Since the total mass and momentum are conserved, $V_{CM} = M_C V_0/(M_C + M_f)$ is constant also, where $M_f = \sum_i m_i, \forall i \notin B$.

The evolution of $V(t)$ in a two-dimensional simulation is shown in Fig. 5(a). After an initial exponential decay, the typical long-time algebraic decay[67,68] $\propto t^{-1}$ is observed which is due to the hydrodynamic self-particle interaction. An enlarged logarithmic plot of the velocity decay is shown in the inset of the figure where the correct algebraic time-dependence can be observed.

TABLE II. Converged resolutions used in the simulation of flow through array of spheres: $dx = dy = dz$, $N_x = N_y = N_z$.

L	7.0	6.0	5.0	4.5	4.0	3.5	3.2	2.8	2.5
dx	0.1	0.1	0.1	0.1	0.1	0.07	0.05925	0.04	0.025
N_x	70	60	50	45	40	50	54	70	100

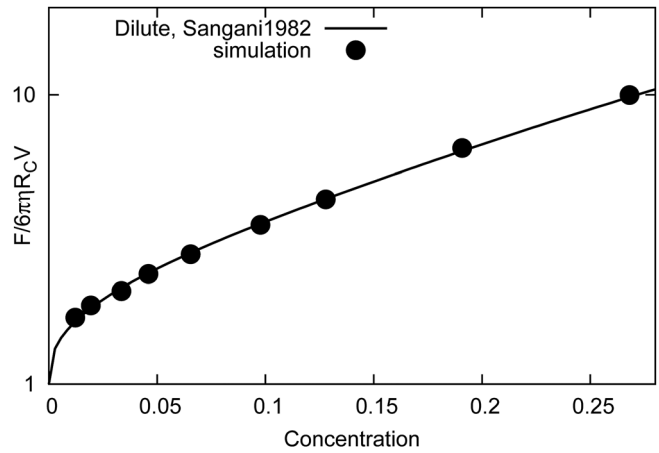

FIG. 4. Three-dimensional dimensionless drag coefficient: comparison with theories of Sangani and Acrivos.[66]

Same arguments apply to the three-dimensional case where the $V(t)$ of the corresponding sphere is shown in Fig. 5(b). Here, algebraic decay is also observed but the scaling is $\propto t^{-3/2}$ in agreement with the theory.[67]

C. A rotating particle under shear flow

As mentioned earlier in Sec. II B, the viscous force formulation adopted in Eq. (7) (formulation A for brevity) does not conserve strictly the angular momentum. We examine the accuracy of torque τ_C acting on a particle by performing two dimensional simulations of a rotating disk under a simple shear flow. The Stokes solution of τ_C in the case of low Reynolds number is given[69] as

$$\tau_C = 4\pi\dot{\gamma}\rho_0\nu R_C^2\left(\frac{1}{2} - \frac{\Omega}{\dot{\gamma}}\right), \tag{15}$$

where $\dot{\gamma}$ is the shear rate and Ω is the angular speed of the disk. The solvent particles are placed at distance with $dx = 0.2$, $\eta = 8.46$; therefore $\nu = \eta/\rho_0 = 8.46$, $C_s = 15.0$. Box size is taken as $L_x = L_y = 20.0$, which is sufficiently large to minimize the wall or periodic image effects. Shear rate between two parallel walls is $\dot{\gamma} = 0.10575$, which defines $Re = \dot{\gamma}R_C^2/\nu = 0.0125$ for the disk. The rotating speeds of the disk are taken as -0.14, -0.07, 0.0, 0.07, 0.14, where "—" means opposite direction of the shear rate. The results are shown in Fig. 6, where formulation A produces incorrect results, and the error of the torque is proportional to the absolute value of the angular speed. We compare the slope of the linear fit for torques at different speeds with the analytical solution. With resolution $dx = 0.2$, the slope has 52% relative error and with a doubled resolution $dx = 0.1$, the error reduces only to 48%. This error does not result from the thin-layer model, since during the rotation the mass of the disk is assumed to be evenly distributed. The discrepancy of

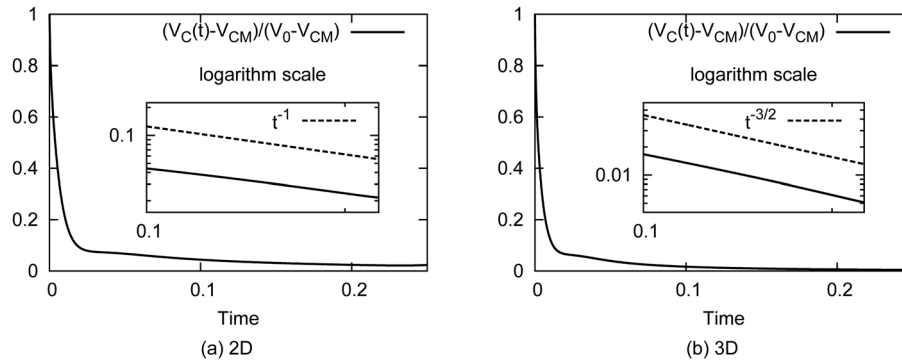

FIG. 5. Algebraical decay of normalized velocity: (a) 2D disk and (b) 3D sphere.

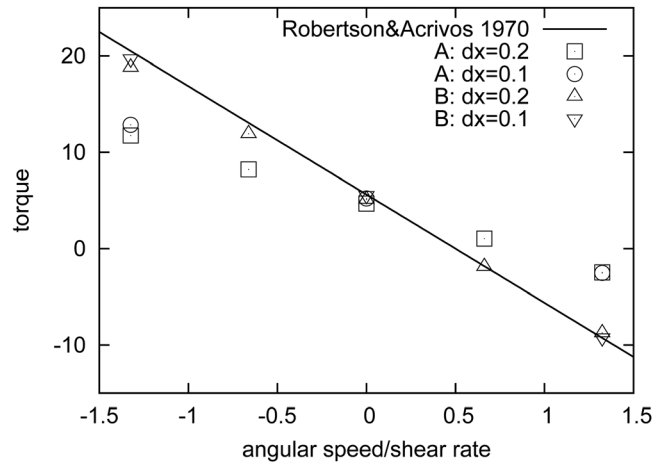

FIG. 6. Torque of a rotating disk under shear flow: formulation A does not conserve angular momentum and produces wrong torque; formulation B conserves angular momentum and produces accurate torque.

the torque should be due to the fact that the viscous force of formulation A is not acting along the center-to-center line between particle pairs; therefore, the angular momentum is not exactly conserved.

The torque may be captured accurately by selecting a type of viscous force acting along the center-to-center line of two particles. We select $F_{ij}^{vis} = 4\eta\left(\frac{1}{d_i^2}+\frac{1}{d_j^2}\right)\frac{\partial W}{\partial r_{ij}}\frac{\mathbf{e}_{ij}\cdot\mathbf{v}_{ij}}{r_{ij}}\mathbf{e}_{ij}$ (formulation B for brevity) from Ref. 70 to replace the viscous force in Eq. (7) and perform the same simulations. The results are also shown in Fig. 6 for comparison, where torque is captured accurately at all rotating speeds, with the error of the slope of linear fit below 3%.

Note that according to FDT viscous formulation B has different expression for thermal fluctuations as counterpart. Formulation B, although improving the results in case of rotating particles, has no effect on their drag. We have explicitly checked this by repeating the simulations presented in Sec. III, obtaining derivations in the results with respect to formulation A below 1%; therefore, the conclusions remain invariant. In the following test cases, standard formulation A will be considered.

D. Hydrodynamic interactions between moving particles

In a concentrated suspension of solid particles, the HIs between them play a crucial role for the macroscopic properties of the bulk system.[71] In this section, we investigate the accuracy of SDPD in describing them. This is an important test case for dynamic simulations of particle suspension, as it can estimate the minimal fluid resolution needed for the correct modeling of the interstitial fluid.

Analytical solutions are available for two spheres defined in a unbounded domain and interacting implicitly through the solvent. In particular, we consider the two following situations: (1) two spheres approaching each other with equal but opposite velocity along their center-to-center line; (2) two spheres moving with relative velocity perpendicular to their center-to-center line.

1. Squeezing motion

Two identical spheres ($R_C^1 = R_C^2 = 1.0$) are immersed in a quiescent solvent characterized by $\nu = 40.0$, $c_s = 400.0$, and $T = 0$. At time $t = 0$, they are forced to start moving with constant velocity magnitude $|\mathbf{V}_x| = 1.0$ towards each other along their center-to-center line until touching. The corresponding Reynolds number $\mathrm{Re} = VR_C/\nu = 2.5 \times 10^{-2}$ and Mach number $\mathrm{Ma} = V/c_s = 2.5 \times 10^{-3}$. A rectangular domain of size $[14, 9, 9]$ is found to be necessary to remove box size effects due to periodic images.

The three-dimensional solution for the drag coefficient $\mathrm{F}_{\|}$ of two nearly touching spheres parallel to their center-to-center line can be obtained by using the method of reflections.[72,73] This is

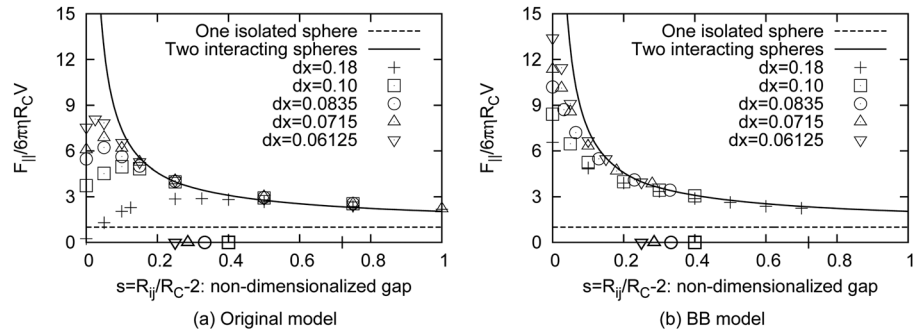

FIG. 7. Drag coefficients vs. gap s between two spheres approaching each other along their center-to-center line (squeezing motion): (a) interactions allowed only through solvent particles; (b) interactions between boundary-boundary particles of different spheres also allowed. The symbols on s axis are r_c corresponding to different resolutions.

plotted in Fig. 7 (solid line) and compared with SDPD simulations for several particle resolutions. Note that for gap distances $s \leq r_c$, kernels centered on boundary particles of different solid spheres could start overlapping and the corresponding SDPD particles could in principle interact.

We consider first the situation where no interaction between different boundary particles is allowed (Fig. 7(a)), and the HIs are mediated uniquely by the solvent. HI are well resolved at moderate inter-particle distances, whereas they start deviating from the theoretical solution as s is getting smaller and eventually they fail completely to recover the expected singular behavior for $s \to 0$. Symbols on the abscissa correspond to the typical cutoff radii r_c used for different resolutions. It can be observed that HI deviate typically for $s \leq r_c/2$, corresponding to less than two fluid particles in the interstitial region along the center-to-center line. At smaller distances, fluid particles in the gap are completely squeezed out, producing smaller repulsive forces and, eventually, depleted layers. Therefore, for two freely moving spheres in a real dynamic simulation, penetration could occur due to absence of any extra force between nearly touching spheres other than the implicit one mediated by the SDPD solvent.

To increase pressure and viscous force between solid particles at small gap distances, we consider the next case in which two boundary particles belonging to different spheres are allowed to interact through the forces described in Eq. (7). Since in this case no specific boundary condition must be enforced, we assign to the boundary particles the "real" rigid body velocity of the corresponding solid structure. This second type of model is denoted for brevity as BB (boundary-boundary). Again, we have performed simulations with different resolutions, and the results are shown in Fig. 7(b). Due to the extra boundary-boundary particle interactions, HIs are recovered up to smaller gap distances and, unlike the previous case, they increase monotonically as decreasing s. This modification introduces extra forces between boundary particles of different spheres which should not be present in a continuum description. However, the range of interaction falls below the typical cutoff radius r_c, and therefore, they can be interpreted as a sub-particle scale lubrication model which prevents penetration. Although improved, the singular behavior is not correctly captured for $s \to 0$. This is, however, not surprising as the interaction forces between particle-pair in Eq. (7) are themselves not singular.

To capture the correct singular behavior at $s \to 0$, either larger resolutions or explicit lubrication corrections could be considered, similar to those presented in Ref. 74, for example, which are, however, limited to spherical particle and do not apply to the arbitrarily shaped objects considered in this work. A more general approach to model the short-range lubrication could be represented by the introduction of extra pair forces between boundary particles belonging to different solid objects with functional form, for example, of the type used in Ref. 36. This approach is currently under investigation and will be presented in a future work.

2. Shear motion

The three-dimensional solution for two spheres moving perpendicular to their center-to-center line is also given in Refs. 72 and 73. Simulations have been performed with two spheres moving

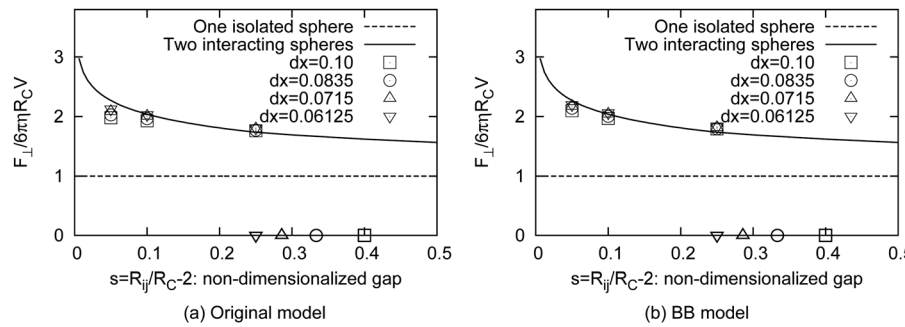

FIG. 8. Drag coefficient vs. gap s between two spheres in opposite motion perpendicular to their center-to-center line (shear motion): (a) interactions through only solvent particles; (b) interactions between boundary-boundary particles of different spheres also allowed. The symbols on s axis are r_c corresponding to different resolutions.

with the same constant velocity magnitude ($|\mathbf{V}_y| = 1.0$) in opposite directions. In this case, box size $[12, 8, 8]$ is considered sufficient to eliminate image effects. Similar to Sec. III D 1, results for two spheres interacting only through solvent particles are shown in Fig. 8(a) for different resolutions. Since for the shear motion considered here there is no squeezing of solvent particles in the gap, good results for $F_\perp$ are obtained up to gap distances $\sim r_c/4$ corresponding to one single SDPD particle only describing the interstitial fluid. Again, slightly better results at smaller distances are achieved by considering extra boundary-boundary particle interactions, see Fig. 8(b).

Note also the much softer logarithmic dependence of $F_\perp$ on s compared to $F_\parallel$ in Fig. 7, suggesting that $F_\parallel$ produced by fluid squeezing between nearly touching spheres should dominate the dynamics for concentrated suspensions.

E. Brownian translation/rotation of solid particle

A micro/nano-sized solid particle is affected by the presence of thermal fluctuations producing its ultimate Brownian diffusive dynamics. In this section, we validate our method for temperature $T \neq 0$ in Eq. (8). A single solid particle is defined in a two/three dimensional domain and its diffusional behavior studied. In particular, we focus on a convergence analysis of its mean square displacements (MSDs) in two-dimensional domain, to understand possible resolution-dependent effects, which provide a guideline for 3D simulations.

1. Brownian disk

A disk of radius $R_c = 1.0$ free to translate and rotate is contained in a periodic square domain of size $L_{x,y} = 5.0$. Fluid solvent is modeled as SDPD particles and characterized by kinematic viscosity $\nu = 15.0$ and thermal energy $k_BT = 1.0$. One such simulation with $t_{end} \approx 340$ is called one realization. To check numerical convergence of the results, three different particle-resolutions are considered: $dx = 0.2$, 0.125, and 0.1.

According to Eq. (9), the maximum variance of solvent thermal velocity (v_{th}^{max}) occurs in the case of highest resolution ($dx = 0.1$). Therefore, we chose the sound speed $c_s \approx 15 v_{th}^{max} = 343.24$ to all the resolutions considered so that a small density variation is obtained. The thermal velocity of the disk is $V_{th} = \sqrt{2k_BT/M_c} = 1.414$; therefore, $Re = V_{th}R_C/\nu = 0.094$ and $Ma = V_{th}/c_s = 0.00412$.

To obtain statistical averages, 50 realizations have been performed for each resolution starting with different random number seed. Velocity probability distribution functions (PDF) for both solvent particles and solid disk satisfy Maxwell-Boltzmann distribution,[47]

$$f(v) = \sqrt{\frac{m}{2\pi k_B T}} exp\left(\frac{-mv^2}{2k_BT}\right). \tag{16}$$

It has been shown that the PDF for solvent particles velocity scales consistently with resolutions while for a solid particle with predefined volume is fixed independent of resolutions.[47]

We check further the diffusive behavior of the disk by calculating its translational and rotational MSD, which are defined as

$$MSD_t(\tau) = \left\langle \mathbf{R}_C^2(t+\tau) - \mathbf{R}_C^2(t) \right\rangle \tag{17}$$

and

$$MSD_r(\tau) = \left\langle \Theta_C^2(t+\tau) - \Theta_C^2(t) \right\rangle, \tag{18}$$

where Θ_C is rotating angle and $\langle\rangle$ is the ensemble average taken over at time t with a time interval τ. The translational MSDs for different resolutions are shown in Fig. 9, where the correct behavior is captured at a rather rough resolution ($dx = 0.2$). The rotational MSDs for different resolutions are plotted in Fig. 10 showing converged results at $dx = 0.125$. Since the momentum of inertia for the disk is fixed for different resolutions, the relative slower convergence of resolution (compared to translation) can be due to the deficiency of torque calculation at low resolution.

The simulations show consistent diffusion behavior for a predefined inclusion as long as the resolution is high enough to calculate force/torque correctly. Due to the connection with SPH, resolution effects, which are somehow difficult to control in DPD methods,[33,40] can be analyzed straightforward in SDPD.

2. Brownian sphere

We performed 15 realizations of a single spherical particle diffusing in a three-dimensional periodic box of size $L_{x,y,z} = 5.0$. We chose $dx = 0.2$, since it is sufficient to capture the translational behavior. All other parameters in these simulations are the same as in the two-dimensional case.

We checked the velocity PDF of solvent particles and compared it with Maxwell-Boltzmann distribution in Fig. 11, where good agreement is obtained. The PDF of the spherical-particle velocity is also validated in Fig. 12.

According to the Einstein-Stokes equation,

$$D_0 = \frac{k_B T}{6\pi\eta R_C}, \tag{19}$$

the diffusion coefficient D_0 of a sphere suspended in an infinite fluid medium can be predicted by the temperature and viscosity of the fluid. If the fluid domain is finite and periodic, the dynamics of the sphere is affected by the complex hydrodynamic interactions with its images. The actual diffusion coefficient D has a correction from D_0 which reads[20]

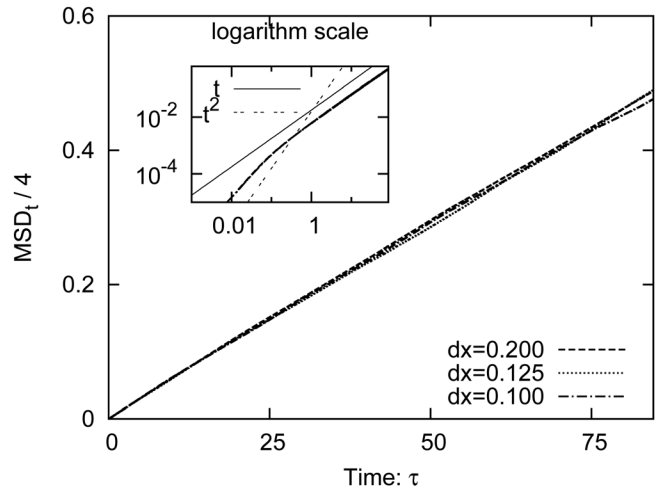

FIG. 9. Convergence of translational mean square displacement for a disk: the slope represents the translational diffusion coefficient in 2D; the inset shows the transition from ballistic to diffusive regime in log-log scale.

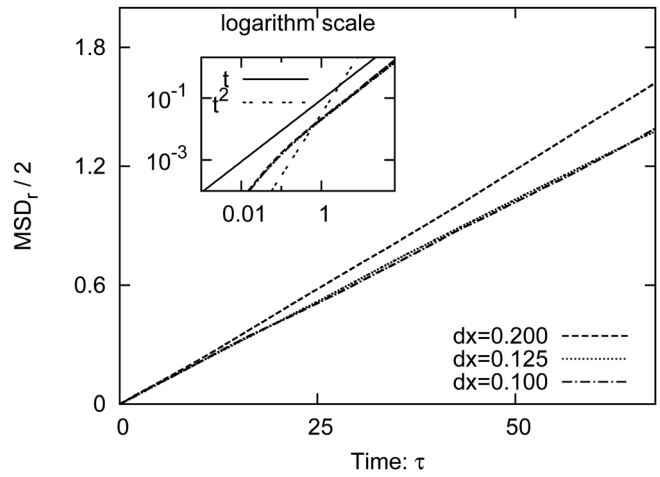

FIG. 10. Convergence of rotational mean square displacement for a disk: the slope represents the rotational diffusion coefficient in 2D; the inset shows the transition from ballistic to diffusive regime in log-log scale.

$$D = \frac{D_0}{\lambda} = \frac{k_B T}{6\pi\eta R_C \lambda}, \tag{20}$$

where λ is the drag coefficient at corresponding concentration of spheres (see Sec. III A. $\lambda \approx 2.15$ in this case).

Analytically, D is related to the translational MSD as

$$D = \frac{1}{6}\lim_{t\to\infty}\frac{d}{dt}(MSD). \tag{21}$$

In Fig. 13, we compare $D_0 t/\lambda$ with the MSD extracted from simulations in a range of sufficiently long time. The linear fit of the MSD in diffusive regime produces a diffusion coefficient with discrepancy to analytical solution smaller than 2%.

F. A colloidal particle near a rigid wall

In this section, we show the ability of the SDPD method to model a particle in the vicinity of an external boundary. The diffusion of a colloidal particle near a flat wall is hindered, as the drag coefficient λ of the particle is enhanced by the complex hydrodynamic interactions. Close to the wall, diffusion D is anisotropic[75] and, therefore, can be split into the motion parallel (along the

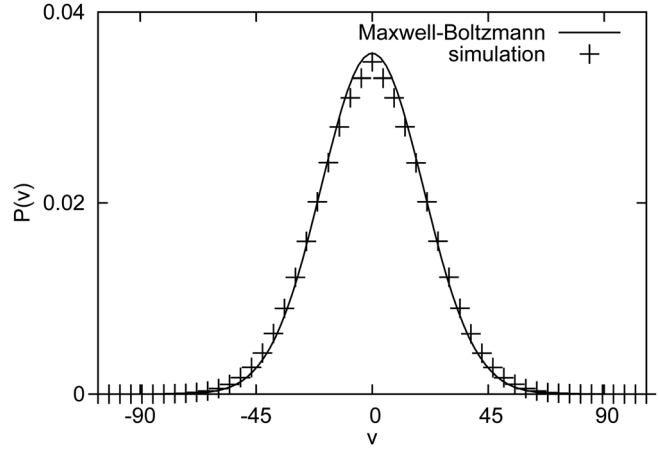

FIG. 11. Probability distribution function for velocity of solvent particles in 3D.

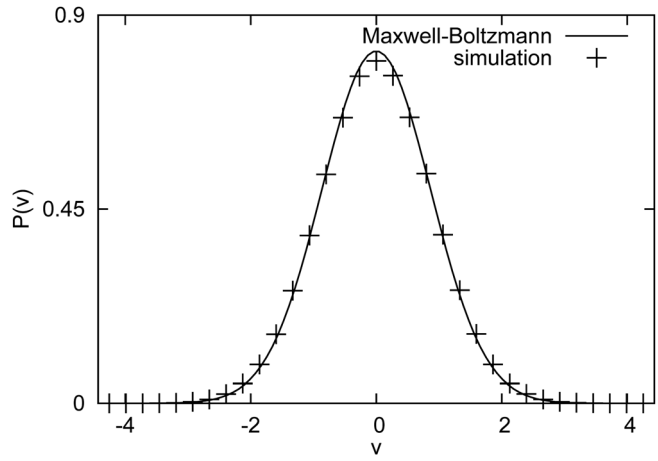

FIG. 12. Probability distribution function for velocity of a sphere in 3D.

plane x, y) and perpendicular (normal to the plane z) to the wall, with both quantities depending on the gap s between the particle surface and the wall, i.e.,

$$\begin{aligned} D_{\perp}(s) &= \frac{D_0}{\lambda_{\perp}(s)} = \frac{1}{2}\lim_{t\to\infty}\frac{d}{dt}(MSD_{\perp}(s)), \\ D_{||}(s) &= \frac{D_0}{\lambda_{||}(s)} = \frac{1}{2}\lim_{t\to\infty}\frac{d}{dt}(MSD_{||}(s)). \end{aligned} \tag{22}$$

The exact solution of $\lambda_{\perp}$ has been given as an infinite series,[76]

$$\lambda_{\perp}(s) = \frac{4}{3}\sinh\alpha\sum_{n=1}^{\infty}\frac{n(n+1)}{(2n-1)(2n+3)}\left[\frac{2\sinh(2n+1)\alpha + (2n+1)\sinh 2\alpha}{4\sinh^2(n+\frac{1}{2})\alpha - (2n+1)^2\sinh^2\alpha} - 1\right], \tag{23}$$

where $\alpha = \cosh^{-1}(1 + s/R_C)$. Without closed analytical form, the $\lambda_{||}$ approximation is derived up to fifth order using the method of reflections,[76]

$$\lambda_{||}(s) \approx 1 - \frac{9}{16}\beta + \frac{1}{8}\beta^3 - \frac{45}{256}\beta^4 - \frac{1}{16}\beta^5 + O(\beta^6), \tag{24}$$

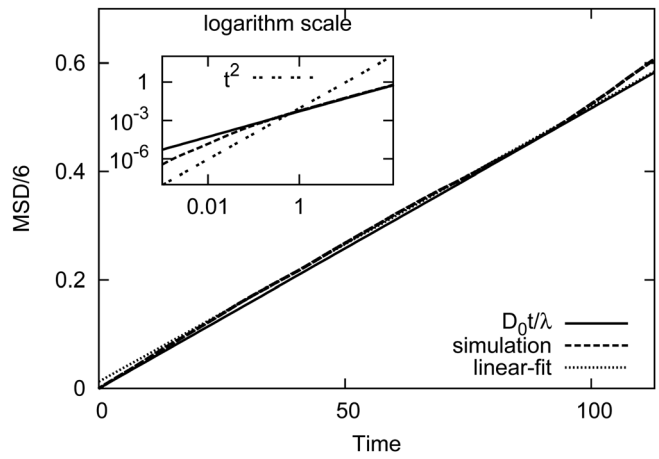

FIG. 13. Comparison of translational mean square displacement of a sphere: the slope represents the translational diffusion coefficient in 3D; the inset shows the transition from ballistic to diffusive regime in log-log scale.

where $\beta = (1 + s/R_C)^{-1}$. Both $\lambda_\perp$ and $\lambda_{||}$ show monotonic increase as the gap s decreases. However, experimental verification of such predictions has been difficult. This is mainly due to the fact that accurate $3D$ trajectories of a sub-micro-sized colloidal particle are difficult to obtain, since the particle may be out of the focal plane of microscopy at any time. Lin *et al.*[11] used optical tweezers to trap the particle location and have a control over s; Carbajal-Tinoco *et al.*[12] found a monotonic relation between the radius of the external ring of the point spread function (PSF) and s, when the fluorescent particle is out of focus. Both of the novel experiments have measured D as a function of s and corroborated the theoretical predictions of Eqs. (23) and (24).

Numerical simulations have no difficulty in this situation, since they record a complete history of the dynamics of the system. We perform a set of SDPD simulations of a sphere near a rigid wall to corroborate Eqs. (23) and (24) and experimental results, meanwhile validate our model of a colloidal particle coupled with an external boundary. A schematic system is illustrated in Fig. 14. A recent similar DPD simulation was performed for the case of a Brownian sphere diffusing between two parallel walls.[77]

Simulations parameters are taken to be the same as in Sec. III E except that the computational domain is increased to be [13, 13, 16] with periodic boundaries in x, y directions and two planar walls in z direction. No-slip boundary conditions as described in Sec. II D are applied at both walls. About 150 realizations have been computed with a spherical particle located at different initial positions Z_C along the direction z normal to the wall. Each Z_C is chosen to be in the vicinity ($Z_C <= 5$) of the bottom wall, which reduces the effect of the upper wall on the results. A post-processing procedure as described in Ref. 12 is adopted, which divides the particle trajectory for each realization into sub-trajectories. Each piece is sufficient long to capture the particle dynamics in the linear diffusive regime. Depending on the initial separations s of each sub-trajectory, ensemble averages of MSD perpendicular/parallel to the wall are calculated, from which $D_\perp(s)$ and $D_{||}(s)$ are extracted.

D_0 is known according to Eq. (19). In Fig. 15, we compare simulation results of $D(s)/D_0$ with Eqs. (23) and (24). Quantitative agreement is achieved except the region very close to the wall ($s < r_c/2$), where hydrodynamic effects can not be fully captured. The density profile using Eq. (5) for the fluid near the wall is averaged over time and shown in the inset of Fig. 15, where fluctuation near the wall is hardly observed.

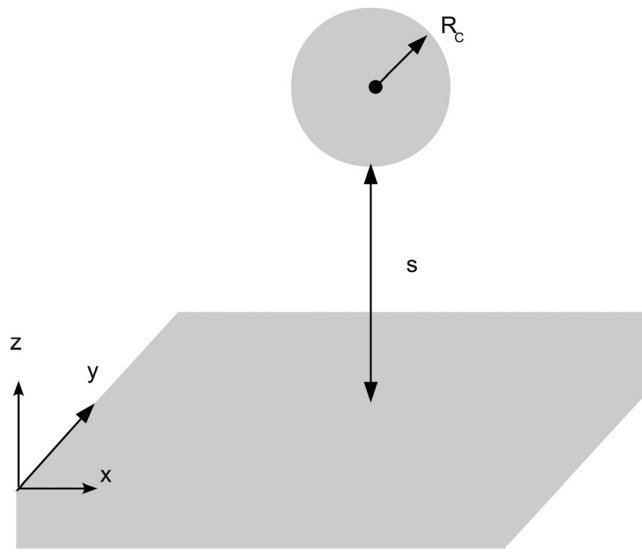

FIG. 14. Scheme of a colloidal particle moving near a rigid plane wall: periodic boundaries in x, y direction and walls in z direction; upper wall is placed sufficiently far; and the diffusion coefficient is anisotropic in perpendicular and parallel directions to the wall.

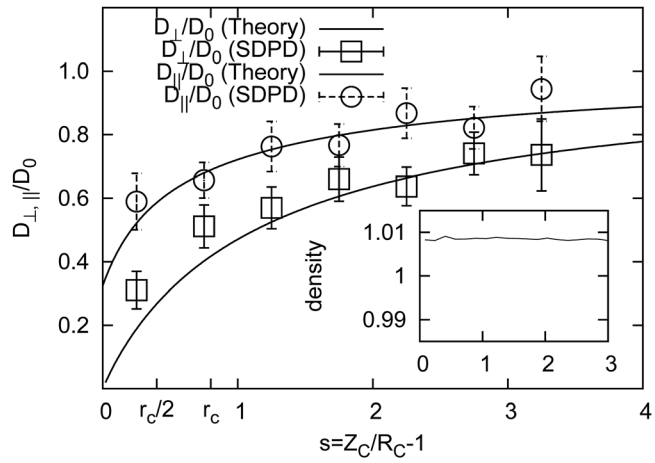

FIG. 15. Diffusion coefficients of a Brownian sphere near a rigid wall: perpendicular and parallel to the wall; the inset shows the normalized fluid density profile averaged over time near the wall.

IV. CONCLUSION

We have presented a model for solid particles in suspension using SDPD.[41] By extending the boundary condition method of Morris *et al.*,[52] particles with general shapes, with arbitrary translation and rotation, can be simulated. With regards to the numerical performance of the present SDPD model, similar to a conventional DPD, the computational cost scales linearly with the total number of suspended solid particles N_C, which is superior to $O(N_C \ln N_C)$ of the accelerated SD (Ref. 16) in number of solid particles. On the other hand, SD takes into account fluid implicitly while SDPD needs to model solvent explicitly. Moreover, the exact representation of the solid particle requires a large number of SDPD boundary particles with consequent increase of the computational cost, which is necessary for description of arbitrarily shaped solid particle. Note that the thin-layer model presented here, by reducing the number of boundary particles to only those lying within a distance r_c from the solid-liquid interface, can speed up dramatically the search of neighboring particles in the cell list, especially in the case of concentrated suspension.

A remark on the comparison of the present model with DPD is in order. The cutoff radius r_c in a SDPD simulation should be $2-4$ times bigger than a typical one used in DPD,[58] with consequent increase in the number of neighbors for each particle and CPU time. This is the price to pay to have an accurate description of the Navier-Stokes equations in the fluid domain. However, this does not prevent us to choose a smaller cutoff radius to reduce the amount of numerical operations, in which case kinetic theory or pre-run would be needed to calibrate the viscosity as in conventional DPD model.

The SDPD particle model presented here has been implemented in the parallel framework of PPM,[61] which is based on message passing interface (MPI) and has communication cost in the order of 10% of the total time by using up to 100 processors, enabling us to run realistic SDPD simulations of particle suspension. Validations ranging from diffusion-dominated regime typical of sub-micro-sized objects towards the non-Brownian regime characterizing macro-continuum flow conditions show good agreement with analytical results. Simulation of anisotropic diffusive behavior of a colloidal particle near a rigid wall has also been performed and validated by analytical solutions.

The development of a lubrication model based on extra "local" pair forces between SDPD boundary particles is currently under investigation and should allow to extend the generality of the current method to the case of concentrated suspensions of arbitrarily shaped objects.

ACKNOWLEDGMENTS

The authors would like to thank the financial support provided by the DFG (German Research Foundation) via Grant No. EL503/1-1 and appreciate discussions with X. Y. Hu and S. Adami. X.B. gratefully acknowledges the support of the TUM-Graduate School's Faculty Graduate Center

Mechanical Engineering at the Technische Universität München. 3D simulations have been mainly performed on National Supercomputer HLRB-II: *SGI Altix 4700* located at Leibniz-Rechenzentrum Garching by Munich, Germany.

[1]J. Mewis and N. J. Wagner, "Current trends in suspension rheology," J. Non-Newtonian Fluid Mech. **157**, 147 (2009).
[2]N. J. Wagner and J. Brady, "Shear thickening in colloidal dispersions," Phys. Today, **62**(10), 27 (2009).
[3]P. Tabeling, *Introduction to Microfluidics*, 2nd ed. (Oxford University Press, Oxford, 2006).
[4]G. E. Karniadakis and A. Beskok, *Microflows and Nanoflows: Fundamentals and Simulation* (Springer, New York, 2005).
[5]M. Pugia, G. Blankenstein, R. Peters, J. Profitt, K. Kadel, T. Willms, R. Sommer, H. Kuo, and L. Schulman, "Microfluidic tool box as technology platform for hand-held diagnostics," Clin. Chem. **51**, 1923 (2005).
[6]W. R. Hwang, M. A. Hulsen, and H. E. H. Meijer, "Direct simulation of particle suspensions in sliding bi-periodic frames," J. Comput. Phys. **194**, 742 (2004).
[7]R. Glowinski, T. Pan, T. Hesla, and D. Joseph, "A distributed Lagrange multiplier fictitious domain method for particulate flows," Int. J. Multiphase Flow **25**, 755 (1999).
[8]N. Patankar, P. Singh, D. Joseph, R. Glowinski, and T. Pan, "A new formulation of the distributed Lagrange multiplier/fictitious domain method for particulate flows," Int. J. Multiphase Flow **26**, 1509 (2000).
[9]Y. Nakayama and R. Yamamoto, "Simulation method to resolve hydrodynamic interactions in colloidal dispersions," Phys. Rev. E **71**, 036707 (2005).
[10]X. Luo, M. R. Maxey, and G. E. Karniadakis, "Smoothed profile method for particulate flows: Error analysis and simulations," J. Comput. Phys. **228**, 1750 (2009).
[11]B. H. Lin, J. Yu, and S. A. Rice, "Direct measurements of constrained Brownian motion of an isolated sphere between two walls," Phys. Rev. E **62**, 3909 (2000).
[12]M. D. Carbajal-Tinoco, R. Lopez-Fernandez, and J. L. Arauz-Lara, "Asymmetry in colloidal diffusion near a rigid wall," Phys. Rev. Lett. **99**, 138303 (2007).
[13]D. Ermak and J. A. McCammon, "Brownian dynamics with hydrodynamic interactions," J. Chem. Phys. **69**, 1352 (1978).
[14]L. Durlofsky, J. F. Brady, and G. Bossis, "Dynamic simulation of hydrodynamically interacting particles," J. Fluid Mech. **180**, 21 (1987).
[15]J. F. Brady and G. Bossis, "Stokesian dynamics," Annu. Rev. Fluid Mech. **20**, 111 (1988).
[16]A. Sierou and J. F. Brady, "Accelerated Stokesian dynamics simulations," J. Fluid Mech. **448**, 115 (2001).
[17]J. W. Swan and J. F. Brady, "Simulation of hydrodynamically interacting particles near a no-slip boundary," Phys. Fluids **19**, 113306 (2007).
[18]R. Kutteh, "Rigid body dynamics approach to Stokesian dynamics simulations of nonspherical particles," J. Chem. Phys. **132**, 174107 (2010).
[19]S. Weinbaum, P. Ganatos, and Z. Yang, "Numerical multipole and boundary integral-equation techniques in Stokes-flow," Annu. Rev. Fluid Mech. **22**, 275 (1990).
[20]N. Sharma and N. A. Patankar, "Direct numerical simulation of the Brownian motion of particles by using fluctuating hydrodynamic equations," J. Comput. Phys. **201**, 466 (2004).
[21]L. D. Landau and E. M. Lifshitz, *Fluid Mechanics*, 2nd ed. (Pergamon, Oxford, 1987).
[22]A. J. C. Ladd, "Numerical simulations of particulate suspensions via a discretized Boltzmann equation. Part 1. Theoretical foundation," J. Fluid Mech. **271**, 285 (1994).
[23]A. J. C. Ladd and R. Verberg, "Lattice-Boltzmann simulations of particle-fluid suspensions," J. Stat. Phys. **104**(5–6), 1191 (2001).
[24]D. L. Koch and A. J. C. Ladd, "Moderate Reynolds number flows through periodic and random arrays of aligned cylinders," J. Fluid Mech. **349**, 31 (1997).
[25]M. A. Van der Hoef, R. Beetstra, and J. A. M. Kuipers, "Lattice-Boltzmann simulations of low-Reynolds-number flow past mono- and bidisperse arrays of spheres: Results for the permeability and drag force," J. Fluid Mech. **528**, 233 (2005).
[26]C. Pan, L. Luo, and C. T. Miller, "An evaluation of lattice Boltzmann schemes for porous medium flow simulation," Comput. Fluids **35**, 898 (2006).
[27]R. S. Maier and R. S. Bernard, "Lattice-Boltzmann accuracy in pore-scale flow simulation," J. Comput. Phys. **229**, 233 (2010).
[28]T. Iwashita and R. Yamamoto, "Short-time motion of Brownian particles in a shear flow," Phys. Rev. E **79**, 031401 (2009).
[29]T. Iwashita and R. Yamamoto, "Direct numerical simulations for non-Newtonian rheology of concentrated particle dispersions," Phys. Rev. E **80**, 061402 (2009).
[30]P. J. Hoogerbrugge and J. M. V. A. Koelman, "Simulating microscopic hydrodynamics phenomena with dissipative particle dynamics," Europhys. Lett. **19**, 155 (1992).
[31]P. Español and P. Warren, "Statistical mechanics of dissipative particle dynamics," Europhys. Lett. **30**, 191 (1995).
[32]J. M. V. A. Koelman and P. J. Hoogerbrugge, "Dynamic simulations of hard-sphere suspensions under steady shear," Europhys. Lett. **21**, 363 (1993).
[33]E. S. Boek, P. V. Conveney, H. N. W. Lekkerkerker, and P. van der Schoot, "Simulating the rheology of dense colloidal suspensions using dissipative particle dynamics," Phys. Rev. E **55**, 3124 (1997).
[34]N. S. Martys, "Study of a dissipative particle dynamics based approach for modeling suspensions," J. Rheol. **49**, 401 (2005).
[35]W. Pan, B. Caswell, and G. E. Karniadakis, "Rheology, microstructure and migration in Brownian colloidal suspensions," Langmuir **26**, 133 (2009).
[36]M. Whittle and K. P. Travis, "Dynamic simulations of colloids by core-modified dissipative particle dynamics," J. Chem. Phys. **132**, 124906 (2010).
[37]C. Marsh, G. Backx, and M. Ernst, "Fokker-Planck-Boltzmann equation for dissipative particle dynamics," Europhys. Lett. **38**, 411 (1997).

[38]J. Backer, C. Lowe, H. Hoefsloot, and P. Iedema, "Combined length scales in dissipative particle dynamics," J. Chem. Phys. **123**, 114905 (2005).
[39]R. Qiao and P. He, "Mapping of dissipative particle dynamics in fluctuating hydrodynamics simulations," J. Chem. Phys. **128**, 126101 (2008).
[40]E. S. Boek and P. van der Schoot, "Resolution effects in dissipative particle dynamics simulations," Int. J. Mod. Phys. C **9**, 1307 (1998).
[41]P. Español and M. Revenga, "Smoothed dissipative particle dynamics," Phys. Rev. E **67**, 026705 (2003).
[42]M. Grmela and H. C. Öttinger, "Dynamics and thermodynamics of complex fluids. I. Development of a general formalism," Phys. Rev. E **56**, 6620 (1997).
[43]H. C. Öttinger and M. Grmela, "Dynamics and thermodynamics of complex fluids. II. Illustrations of a general formalism," Phys. Rev. E **56**, 6633 (1997).
[44]J. J. Monaghan, "Smoothed particle hydrodynamics," Annu. Rev. Astron. Astrophys. **30**, 543 (1992).
[45]J. J. Monaghan, "Smoothed particle hydrodynamics," Rep. Prog. Phys. **68**, 1703 (2005).
[46]P. Español, M. Serrano, and H. C. Öttinger, "Thermodynamically admissible form for discrete hydrodynamics," Phys. Rev. Lett. **83**, 4542 (1999).
[47]A. Vázquez-Quesada, M. Ellero, and P. Español, "Consistent scaling of thermal fluctuations in smoothed dissipative particle dynamics," J. Chem. Phys. **130**, 034901 (2009).
[48]S. Litvinov, M. Ellero, X. Y. Hu, and N. A. Adams, "Smoothed dissipative particle dynamics model for polymer molecules in suspension," Phys. Rev. E **77**, 066703 (2008).
[49]S. Litvinov, M. Ellero, X. Y. Hu, and N. A. Adams, "Particle-layering effect in wall-bounded dissipative particle dynamics," Phys. Rev. E **82**, 066704 (2010).
[50]X. Y. Hu and N. A. Adams, "A multi-phase SPH method for macroscopic and mesoscopic flows," J. Comput. Phys. **213**, 844 (2006).
[51]A. Vázquez-Quesada, M. Ellero, and P. Español, "Smoothed particle hydrodynamic model for viscoelastic fluids with thermal fluctuations," Phys. Rev. E **79**, 056707 (2009).
[52]J. P. Morris, P. J. Fox, and Y. Zhu, "Modeling low Reynolds number incompressible flows using SPH," J. Comput. Phys. **136**, 214 (1997).
[53]A. S. Khair and J. F. Brady, "Microrheology of colloidal dispersions: Shape matters," J. Rheol. **52**, 165 (2008).
[54]G. K. Batchelor, *An Introduction to Fluid Dynamics* (Cambridge University Press, Cambridge, UK, 1967).
[55]J. J. Monaghan, "Simulating free surface flows with SPH," J. Comp. Phys. **110**, 399 (1994).
[56]M. Ellero and N. A. Adams, "SPH simulations of flow around a periodic array of cylinders confined in a channel," Int. J. Numer. Methods Eng. **86**, 1027 (2011).
[57]N. J. Quinlan, M. Basa, and M. Lastiwka, "Truncation error in mesh-free particle methods," Int. J. Numer. Methods Eng. **66**, 2064 (2006).
[58]R. D. Groot and P. B. Warren, "Dissipative particle dynamics: Bridging the gap between atomistic and mesoscopic simulation," J. Chem. Phys. **107**, 4423 (1997).
[59]S. Chen, N. Phan-Thien, B. C. Khoo, and X. J. Fan, "Flow around spheres by dissipative particle dynamics," Phys. Fluids **18**, 103605 (2006).
[60]R. Courant, K. Friedrichs, and H. Lewy, "Über did partiellen Differenzengleichungen der mathematicshcen Physik," Math. Ann. **100**, 32 (1928).
[61]I. F. Sbalzarini, J. H. Walther, M. Bergdorf, S. E. Hieber, E. M. Kotsalis, and P. Koumoutsakos, "PPM—A highly efficient parallel particle-mesh library for the simulation of continuum systems," J. Comput. Phys. **215**, 566 (2006).
[62]J. T. Padding and A. A. Louis, "Hydrodynamic interactions and Brownian forces in colloidal suspensions: Coarse-graining over time and length scales," Phys. Rev. E **74**, 031402 (2006).
[63]H. Hasimoto, "On the periodic fundamental solutions of the Stokes equations and their application to viscous flow past a cubic array of spheres," J. Fluid Mech. **5**, 317 (1959).
[64]A. S. Sangani and A. Acrivos, "Slow flow past periodic array of cylinders with application to heat transfer," Int. J. Multiphase Flow **8**, 193 (1982).
[65]Y. Zhu, P. J. Fox, and J. P. Morris, "A pore-scale numerical model for flow through porous media," Int. J. Numer. Analyt. Meth. Geomech. **23**, 881 (1999).
[66]A. S. Sangani and A. Acrivos, "Slow flow through a periodic array of spheres," Int. J. Multiphase Flow **8**, 343 (1982).
[67]B. J. Alder and T. E. Wainwright, "Decay of the velocity autocorrelation function," Phys. Rev. A **1**, 18 (1970).
[68]M. H. Hagen, I. Pagonabarraga, C. P. Lowe, and D. Frenkel, "Algebraic decay of velocity fluctuations in a confined fluid," Phys. Rev. Lett. **78**, 3785 (1997).
[69]C. R. Robertson and A. Acrivos, "Low Reynolds number shear flow past a rotating circular cylinder. Part 1. Momentum transfer," J. Fluid Mech. **40**(4), 685 (1970).
[70]X. Y. Hu and N. A. Adams, "Angular-momentum conservative smoothed particle hydrodynamics for incompressible viscous flows," Phys. Fluids **18**, 101702 (2006).
[71]G. K. Batchelor, "The determination of the bulk stress in a suspension of spherical particles to order c^2," J. Fluid Mech. **56**, 401 (1972).
[72]D. J. Jeffrey and Y. Onishi, "Calculation of the resistance and mobility functions for two unequal rigid spheres in low-Reynolds-number flow," J. Fluid. Mech. **139**, 261 (1984).
[73]S. Kim and S. J. Karrila, *Microhydrodynamics: Principles and Selected Applications* (Butterworth-Heinemann, Boston, MA, 1991).
[74]N. Q. Nguyen and A. J. C. Ladd, "Lubrication corrections for lattice-Boltzmann simulations of particle suspensions," Phys. Rev. E **66**, 046708 (2002).
[75]S. Jeney, B. Lukić, J. A. Kraus, T. Franosch, and L. Forró, "Anisotropic memory effects in confined colloidal diffusion," Phys. Rev. Lett. **100**, 240604 (2008).
[76]J. Happel and H. Brenner, *Low Reynolds Number Hydrodynamics with Special Applications to Particulate Media* (Martinus Nijhoff, The Hague, 1983).
[77]Z. Li and G. Drazer, "Hydrodynamic interaction in dissipative particle dynamics," Phys. Fluids **20**, 103601 (2008).